p53 constrains progression to anaplastic thyroid carcinoma in a *Braf*-mutant mouse model of papillary thyroid cancer

David G. McFadden[a,b], Amanda Vernon[a], Philip M. Santiago[a], Raul Martinez-McFaline[a], Arjun Bhutkar[a], Denise M. Crowley[a], Martin McMahon[c], Peter M. Sadow[d], and Tyler Jacks[a,1]

[a]Koch Institute for Integrative Cancer Research and Department of Biology, Massachusetts Institute of Technology, Cambridge, MA 02142; [b]Endocrine/Thyroid Unit and Department of Medicine, and [d]Department of Pathology, Massachusetts General Hospital, Harvard Medical School, Boston, MA 02114; and [c]Department of Cell and Molecular Pharmacology, Helen Diller Family Comprehensive Cancer Center, University of California, San Francisco, CA 94122

Contributed by Tyler Jacks, March 18, 2014 (sent for review December 12, 2013)

Anaplastic thyroid carcinoma (ATC) has among the worst prognoses of any solid malignancy. The low incidence of the disease has in part precluded systematic clinical trials and tissue collection, and there has been little progress in developing effective therapies. *v-raf murine sarcoma viral oncogene homolog B* (*BRAF*) and *tumor protein p53* (*TP53*) mutations cooccur in a high proportion of ATCs, particularly those associated with a precursor papillary thyroid carcinoma (PTC). To develop an adult-onset model of *BRAF*-mutant ATC, we generated a thyroid-specific CreER transgenic mouse. We used a Cre-regulated $Braf^{V600E}$ mouse and a conditional *Trp53* allelic series to demonstrate that p53 constrains progression from PTC to ATC. Gene expression and immunohistochemical analyses of murine tumors identified the cardinal features of human ATC including loss of differentiation, local invasion, distant metastasis, and rapid lethality. We used small-animal ultrasound imaging to monitor autochthonous tumors and showed that treatment with the selective BRAF inhibitor PLX4720 improved survival but did not lead to tumor regression or suppress signaling through the MAPK pathway. The combination of PLX4720 and the mapk/Erk kinase (MEK) inhibitor PD0325901 more completely suppressed MAPK pathway activation in mouse and human ATC cell lines and improved the structural response and survival of ATC-bearing animals. This model expands the limited repertoire of autochthonous models of clinically aggressive thyroid cancer, and these data suggest that small-molecule MAPK pathway inhibitors hold clinical promise in the treatment of advanced thyroid carcinoma.

vemurafenib | anaplastic thyroid cancer | MEK inhibitor | genetically-engineered mouse model

Mutations in the v-raf murine sarcoma viral oncogene homolog B (BRAF) kinase occur in ∼60% of papillary thyroid carcinomas (PTCs) (www.cbioportal.org/public-portal/data_sets.jsp). PTC generally exhibits an excellent prognosis with conventional therapy, including surgery and selective use of radioiodine (1). PTC may progress to clinically aggressive forms of thyroid cancer, including poorly differentiated thyroid carcinoma (PDTC), which exhibits more rapid growth and poorer clinical outcome. Less commonly, PTC progresses to undifferentiated (anaplastic) thyroid carcinoma (ATC) that is associated with a grim prognosis with a median survival of 5 mo and a 1-y survival of only 20% (2).

Focused sequencing of clinically aggressive subsets of thyroid cancers including PDTC and ATC suggests acquired cooperating mutations drive thyroid cancer progression (3, 4). Mutations in *tumor protein p53* (*TP53*) occur with increasing frequency in more aggressive forms of thyroid cancer, culminating in ATC, which harbors the highest frequency of *TP53* mutations (5–7). ATC may progress from well-differentiated thyroid carcinomas and is also believed to arise spontaneously, possibly from clinically undetectable microscopic well-differentiated thyroid tumors. In the former scenario, ATCs frequently harbor mutations in *BRAF*, and these mutations are concordant between the anaplastic and papillary components. This implicates *BRAF* mutation as an initiating somatic genetic event and supports the hypothesis that loss of p53 function is important for progression to ATC (3, 8).

Mouse models of thyroid cancer have supported the model of acquired mutations driving tumor progression. Although each study has technical limitations, including embryonic oncogene expression and/or elevated circulating thyroid-stimulating hormone (TSH) levels, this work generally supports the notion that $BRAF^{T1799A}$ is sufficient to initiate PTC (9–12). In addition, deletion of p53 enabled tumor progression to high-grade thyroid carcinomas in a transgenic mouse model of translocations targeting the ret proto-oncogene (*RET/PTC*) driven PTC, and a model of follicular thyroid carcinoma initiated by tissue-specific *phosphatase and tensin homolog* (*Pten*) deletion (13, 14). These studies provide functional evidence of an important tumor suppressive role for p53 during thyroid carcinoma progression, although to date this has not been tested in models of *BRAF*-mutant PTC.

Given the high frequency of *BRAF* and *RAS* mutations in thyroid carcinomas and the success of targeted therapy trials for advanced thyroid cancers, the potential utility of small-molecule inhibitors of the MAPK pathway has garnered much recent attention (15). These drugs have also been studied in models of *BRAF*-mutant thyroid carcinoma. Initial observations using a thyroid-specific doxycycline-inducible $BRAF^{T1799A}$ allele suggested that BRAF or mapk/Erk kinase (MEK) inhibition induced thyroid

Significance

We generated a thyroid-specific CreER transgenic mouse and used this strain to model progression of *v-raf murine sarcoma viral oncogene homolog B* (*BRAF*)-mutant papillary thyroid cancer to anaplastic thyroid cancer (ATC). These murine tumors recapitulated the temporal progression and molecular hallmarks of human ATC. We demonstrated that combined mapk/Erk kinase (MEK) and BRAF inhibition resulted in enhanced antitumor activity vs. single-agent BRAF inhibitors in this preclinical model. This model represents a previously lacking mouse model of *BRAF*-mutant ATC and adds to the experimental armamentarium of a highly lethal disease in need of scientific advances. These data also suggest that potent inhibition of the MAPK pathway may improve outcomes in advanced thyroid cancers.

Author contributions: D.G.M. and T.J. designed research; D.G.M., A.V., P. M. Santiago, R.M.-M., and D.M.C. performed research; M.M. contributed new reagents/analytic tools; D.G.M., A.B., and P. M. Sadow analyzed data; and D.G.M. wrote the paper.

The authors declare no conflict of interest.

Data deposition: The data reported in this paper have been deposited in the Gene Expression Omnibus (GEO) database, www.ncbi.nlm.nih.gov/geo (accession no. GSE55933).

[1]To whom correspondence should be addressed. E-mail: tjacks@mit.edu.

This article contains supporting information online at www.pnas.org/lookup/suppl/doi:10.1073/pnas.1404357111/-/DCSupplemental.

carcinoma regression and differentiation (9). However, a recent study from the same laboratory showed a mitigated response to BRAF (PLX4032, vemurafenib) inhibition in human papillary and ATC cell lines and in an endogenous $Braf^{V600E}$-driven PTC mouse model. In response to PLX4032/vemurafenib, feedback inhibition of the human epidermal growth factor receptor 3 (HER3) receptor tyrosine kinase was abrogated, leading to reactivation of MAPK signaling (16). In addition, responses in patients treated with the BRAF inhibitor vemurafenib have exhibited modest activity (17).

To develop an adult-onset autochthonous model of clinically aggressive thyroid carcinoma, we generate a thyroid-specific CreER transgenic mouse and use conditional $Braf^{T1799A}$ and *Trp53* alleles. We demonstrate that expression of $BRAF^{V600E}$ is sufficient to initiate tumorigenesis in adult animals, and p53 loss enables progression to bona fide ATC recapitulating the cardinal features of the human disease including intrinsic resistance to BRAF inhibitors.

Results

$Braf^{V600E}$ Initiates PTC in the Adult Murine Thyroid. To model adult-onset thyroid cancer with Cre-regulated alleles in genetically engineered mice, we first generated and characterized a thyrocyte-specific CreER transgenic mouse using a well-characterized thyroid specific promoter construct (18). We generated two independent transgenic *TPOCreER* lines, each of which behaved similarly with respect to tamoxifen dependence (Fig. S1 *B–E*). *TPOCreER* animals were crossed to a Cre-inducible oncogenic $Braf^{V600E}$ allele, $Braf^{CA}$ (Fig. S1*A*) (19). Several weeks after administration of tamoxifen, *TPOCreER;* $Braf^{CA/+}$ (referred to as TB) animals developed PTC in a tamoxifen-dependent manner (Fig. 1*A* and Fig. S1 *D* and *E*; 12 wk postinduction). This is similar to a previously described *TgCreER* allele, although the *TPOCreER* allele appears to exhibit less tamoxifen independence (10). TB tumors displayed both papillary growth morphology and nuclear features of PTC and exhibited increased phospho-Erk staining by immunohistochemistry (IHC) (Fig. 1*A* and Fig. S1 *E–G*). Even with very long latency (>12–16 mo), extrathyroidal invasion was not observed, and cervical lymph node metastases were not identified in PTC-bearing animals, suggesting that either additional acquired events are necessary in addition to *Braf* mutation, or micrometastatic nodal disease exists below the sensitivity of our detection. A single tamoxifen-treated TB animal (of over 50 animals) developed an invasive carcinoma with spindle cell pattern, consistent with ATC, and another animal (with tall cell and columnar cell features in the primary tumor) had detectable lung metastases upon necropsy. Tumor-bearing TB animals exhibited decreased survival relative to controls. However, given the long survival of PTC-bearing animals that approached the wild-type murine lifespan, this was not statistically significant (Fig. 1*G*; $P = 0.2600$). In addition, these animals generally succumbed to respiratory compromise as a result of large noninvasive tumors causing extrinsic tracheal compression.

We independently confirmed the sufficiency of $Braf^{V600E}$ to initiate PTC in the adult murine thyroid by surgical delivery of Cre-expressing adenovirus to the adult murine thyroid gland. $Braf^{CA/+}$animals at 8–12 wk of age underwent surgical delivery of a single unilateral injection 1uL of Ad5-CMV-Cre into the thyroid parenchyma. Four of six animals harbored PTCs several months following tumor initiation, consistent with results from the TB animals (Fig. S1*H*).

p53 Loss Enables Progression to ATC. Because *TP53* mutations are more common in aggressive subtypes of human thyroid carcinoma, we crossed TB mice to conditional *Trp53* alleles to accelerate disease progression (Fig. S1*A*). Tamoxifen-treated *TPOCreER;* $Braf^{CA/+}$*;* $Trp53^{LSL\text{-}R270H/+}$ developed large PTCs that exhibited histologic features associated with clinically aggressive behavior, including solid growth, tall cell morphology, focal necrosis, and hobnail features (Fig. 1*B*). In addition, ~50% of these animals acquired PDTC or ATC and exhibited significantly shortened survival relative to *TPOCreER;* $Braf^{CA/+}$ animals (Fig. 1*G*; $P < 0.0001$).

Homozygous deletion of p53 (*TPOCreER;* $Braf^{CA/+}$*;* $Trp53^{\Delta ex2\text{-}10/\ \Delta ex2\text{-}10}$, referred to as TBP) or expression of point mutant p53 with conditional loss of the wild-type allele (*TPOCreER;* $Braf^{CA/+}$*;* $Trp53^{LSL\text{-}R270H/\ \Delta ex2\text{-}10}$) further accelerated disease progression to PDTC and overt ATC (Fig. 1 *C–E*) with a median survival of ~6 mo following tumor induction (Fig. 1*G*; $P < 0.0001$; TBP vs. TB animals). These animals quickly deteriorated after progression to ATC, with rapidly growing neck masses and development of audible respiratory stridor (referred to as mATC for murine ATC). Histologic analysis confirmed the presence of undifferentiated (anaplastic) thyroid carcinoma with highly pleomorphic, atypical cells with evidence of necrosis, tracheal invasion, and extrathyroidal extension (Fig. 1 *D* and *E*). We did not discern differences in the histopathology of p53 null ($Trp53^{\Delta ex2\text{-}10/\ \Delta ex2\text{-}10}$) vs. p53 mutant ($Trp53^{LSL\text{-}R270H/\ \Delta ex2\text{-}10}$) tumors. Although mutant p53 caused a slight acceleration of progression (mean survival 181 d vs. 236 d; $P = 0.0121$), these experiments were not specifically designed to control for tamoxifen dose or genetic background; therefore, additional cohorts of littermate animals would be necessary to confirm acceleration of the model by mutant p53. The predominant histologic pattern of ATC in both genotypes was spindle cell, with pleomorphic giant cell pattern also being frequently observed (Fig. 2*A*).

We did not detect regional lymph node metastases, and macroscopic lung metastases were identified in a minority of TBP animals. Because lung metastases are common in human ATC, we examined histological sections from the lungs of 26 mATC-bearing animals and identified microscopic metastases in 5/26 animals (19%) (Fig. 1*F*). This may suggest that hematogenous dissemination occurs following transformation from papillary to anaplastic carcinoma, although additional studies will be necessary to establish the timing of metastatic seeding. It is likely that the natural history of untreated mATC leads to high mortality from local disease progression and precludes the development of macroscopic pulmonary disease in most animals.

mATCs Exhibit the Molecular Hallmarks and Explosive Growth of Human ATC. We performed immunohistochemical studies with markers of thyroid differentiation to confirm thyroid epithelial origin. Low-level expression of the thyroid master regulator Nkx2-1/TTF-1 and cytokeratin 8 (CK8) expression confirmed thyroid epithelial features (Fig. 2 *D* and *E*). In contrast, markers of medullary thyroid carcinoma (chromogranin A; Fig. 2*B*), and rhabdomyosarcoma (including desmin; Fig. 2*C*) were absent in these tumors. These results are consistent with thyroid epithelial origin of mATC. In the p53 mutant model ($Trp53^{LSL\text{-}R270H/\ \Delta ex2\text{-}10}$), p53 protein was stabilized only in the ATC compartment, suggesting that the cellular signals impinging on p53 are activated uniquely in ATC cells (Fig. 2*F*).

We also used small-animal ultrasound to monitor the temporal dynamics of tumor progression in the TBP model. Tumors exhibited very slow initial growth upon tumor induction; however, serial ultrasound monitoring of tumors showed rapid tumor growth in TBP animals after a variable latency, and histology confirmed ATC in these lesions (Fig. 2 *G–I*). mATC and mPTC components were easily discriminated by ultrasound characteristics: mATC exhibited a more uniform, hypoechoic appearance, whereas mPTC were heterogeneous and often partially cystic lesions. Serial measurement of tumor area in these animals demonstrated the sudden conversion and rapid growth of ATC in the TBP model, mimicking the explosive growth of human ATC (Fig. 2*J*).

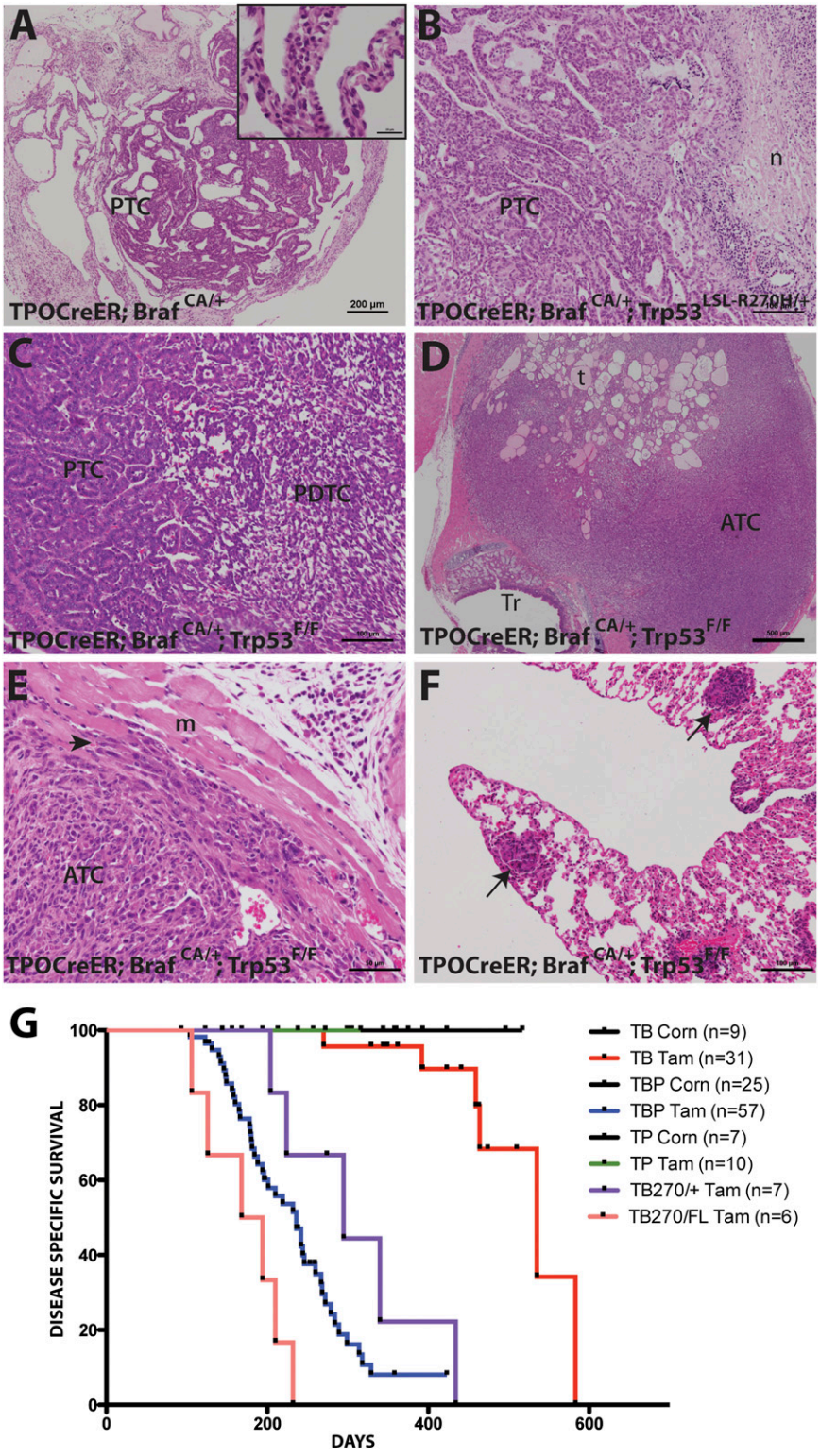

Fig. 1. p53 loss and mutation accelerate progression to PDTC and undifferentiated thyroid carcinoma. (*A*–*F*) H&E histological sections of tamoxifen-treated *TPOCreER; Braf*^{CA} animals crossed to Trp53 alleles. (*A*) *TPOCreER; Braf*$^{CA/+}$ animal acquires PTC demonstrating papillary growth (*Inset*). (*B*) *TPOCreER; Braf*$^{CA/+}$*; Trp53*$^{LSL\text{-}R270H/+}$ thyroid exhibiting PTC with focal necrosis. (*C*) *TPOCreER; Braf*$^{CA/+}$*; Trp53*$^{F/F}$ animal with PTC transitioning to PDTC. (*D*) Low-power view *TPOCreER; Braf*$^{CA/+}$*; Trp53*$^{F/F}$ animal showing large ATC invading through normal thyroid and abutting the trachea. (*E*) Extrathyroidal muscle invasion in *TPOCreER; Braf*$^{CA/+}$*; Trp53*$^{F/F}$ animal (arrowhead). (*F*) Multiple microscopic lung metastases in *TPOCreER; Braf*$^{CA/+}$*; Trp53*$^{F/F}$ animal (arrows). (*G*) Kaplan–Meier curves of TBP allelic series animals including TB, *TPOCreER; Braf*$^{CA/+}$*; Trp53*$^{F/F}$ (TBP), *TPOCreER; Braf*$^{CA/+}$*; Trp53*$^{LSL\text{-}R270H/+}$ (TB270/+), and *TPOCreER; Braf*$^{CA/+}$*; Trp53*$^{LSL\text{-}R270H/FL}$ (TB270/FL). m, muscle; n, necrosis; NL, normal thyroid; t, thyroid; Tr, trachea.

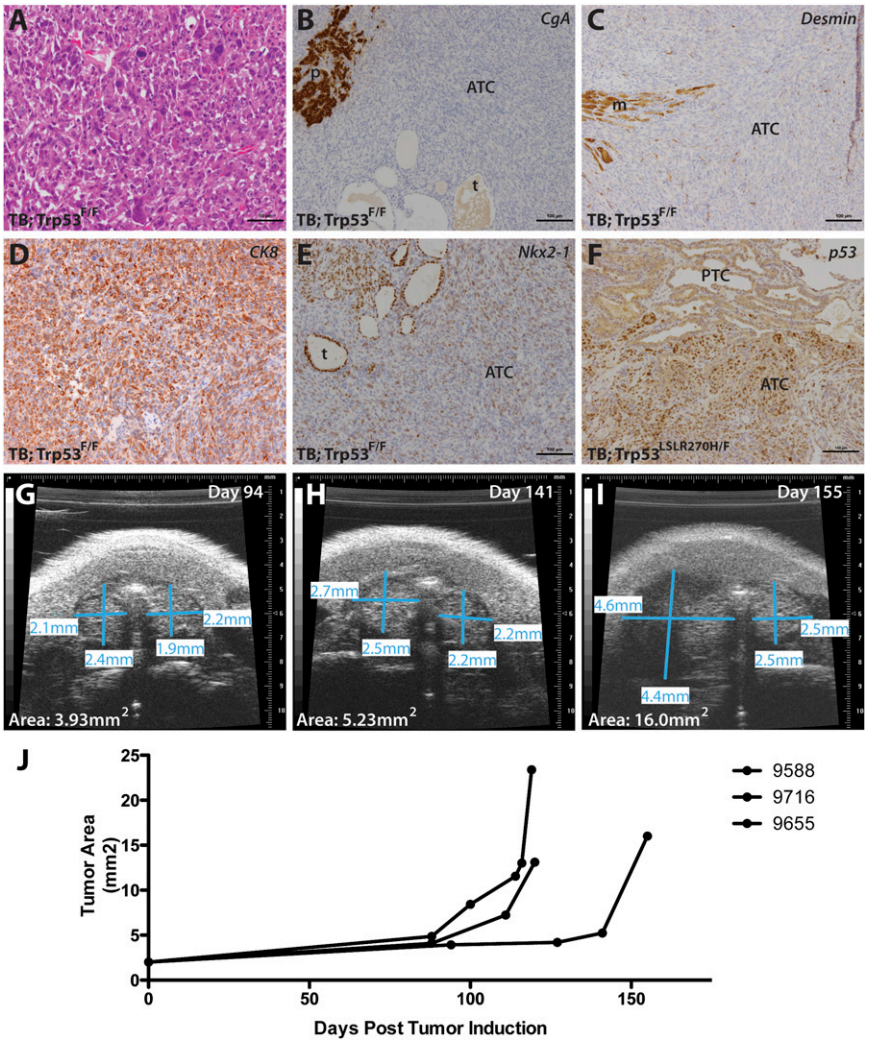

Fig. 2. TBP mATC exhibits histological features and growth dynamics of human ATC. (*A–F*) Histological analysis of mATC. (*A*) H&E staining of TBP mATC showing pleomorphic giant cell subtype. (*B*) Anti-chromogranin A (CgA) staining shows positive staining in a parathyroid gland and negative staining in mATC cells. (*C*) Anti-desmin IHC demonstrating focal positive staining in muscle and myofibroblasts. (*D*) Positive anti-CK8 IHC in mATC cells. (*E*) Anti-Nkx2-1/TTF1 staining showing positive staining in normal thyroid follicular epithelial cells and weak staining in mATC cells. (*F*) Anti-p53 IHC in TB; *Trp53*$^{LSLR270H/F}$ tumor demonstrating mutant p53 stabilization in ATC compartment. (*G–I*) Serial small-animal ultrasound images showing explosive growth of ATC after long initial latency. Tumor area, shown at lower left, was calculated based on cross sectional measurements. (*J*) Chart of tumor area of three tamoxifen-treated TBP animals by serial ultrasound imaging highlighting the rapid onset of ATC with explosive growth. p, parathyroid; t, normal thyroid.

Progression to ATC Is Independent of Circulating TSH. Circulating TSH secreted by the anterior pituitary is a known growth factor for thyrocytes and thyroid carcinoma cells, and activation of the MAPK pathway has been shown to impair thyroid hormone biogenesis leading to compensatory TSH elevation and acceleration of disease progression in mouse PTC models (10–12, 20). Therefore, we measured TSH following induction of Braf^{V600E} in these models. In contrast to previously published models in which TSH was elevated ∼1000 fold, we detected a less than 10-fold elevation of TSH in tumor-bearing animals (Fig. 3*A*). This most likely results from the mosaic activity of the TPOCreER transgene in the follicular epithelium (Fig. S1*C*). To conclusively exclude a requirement for supraphysiologic TSH signaling in disease progression, we added supraphysiologic levels of L-thyroxine to the water of a cohort of TBP animals immediately following tamoxifen administration and completely suppressed TSH (Fig. 3*A*). These animals also developed ATCs with a similar histology and latency as untreated controls (Fig. 3*B*; $P = 0.0896$), confirming that TSH stimulation is not a necessary component of disease progression to ATC in this model.

Murine ATCs Exhibit a Gene Expression Profile of High-Grade, Undifferentiated Carcinomas. To begin to define the molecular events that discriminate murine PTC and ATC, we performed gene expression profiling with Affymetrix Gene 1.0 ST arrays on five TB tumors and four TBP tumors (Dataset S1, Table S1).

Gene-set enrichment analysis (GSEA) was used to compare global gene expression patterns in mPTC and mATC (21). Using a false-discovery rate of less than 25% and $P < 0.01$, we identified 411 differentially up-regulated and 178 down-regulated gene sets in mATC compared with mPTC. Differentially expressed gene sets included signatures of cellular proliferation, consistent with the rapid growth observed by ultrasound monitoring. In addition, signatures of PDTC and ATC were up-regulated in mATC (Fig. 4*A* and Dataset S1, Table S3). Epithelial gene expression signatures were down-regulated in TBP tumors, consistent with epithelial-to-mesenchymal transition (EMT) during progression from PTC to ATC. Genes down-regulated in metastatic vs. primary melanomas were also down-regulated mATC vs. mPTC, consistent with the increase in tumor grade and frequency of

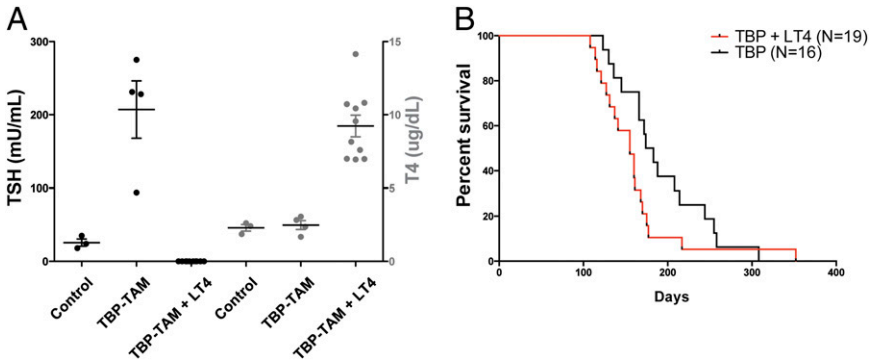

Fig. 3. Progression to mATC is independent of circulating TSH. (*A*) Serum thyroid function testing in mATC animal cohorts. TSH level (mU/mL) shown on the left *y* axis and shown in black; T4 levels (μg/dL) shown on right *y* axis and depicted in gray. Control animals exhibit normal TSH and T4 levels. Tamoxifen-treated TBP animals show elevated TSH but normal T4 levels. Tamoxifen-treated TBP animals supplemented with L-thyroxine (5 μg/mL in drinking water) show undetectable TSH and elevated T4 levels. (*B*) Kaplan–Meier plot of L-thyroxine supplemented vs. control TBP animal survival.

metastases noted in the TBP model (Fig. 4*B* and Dataset S1, Table S4).

Manual examination of differentially expressed genes is also consistent with prior hypotheses of anaplastic transformation.

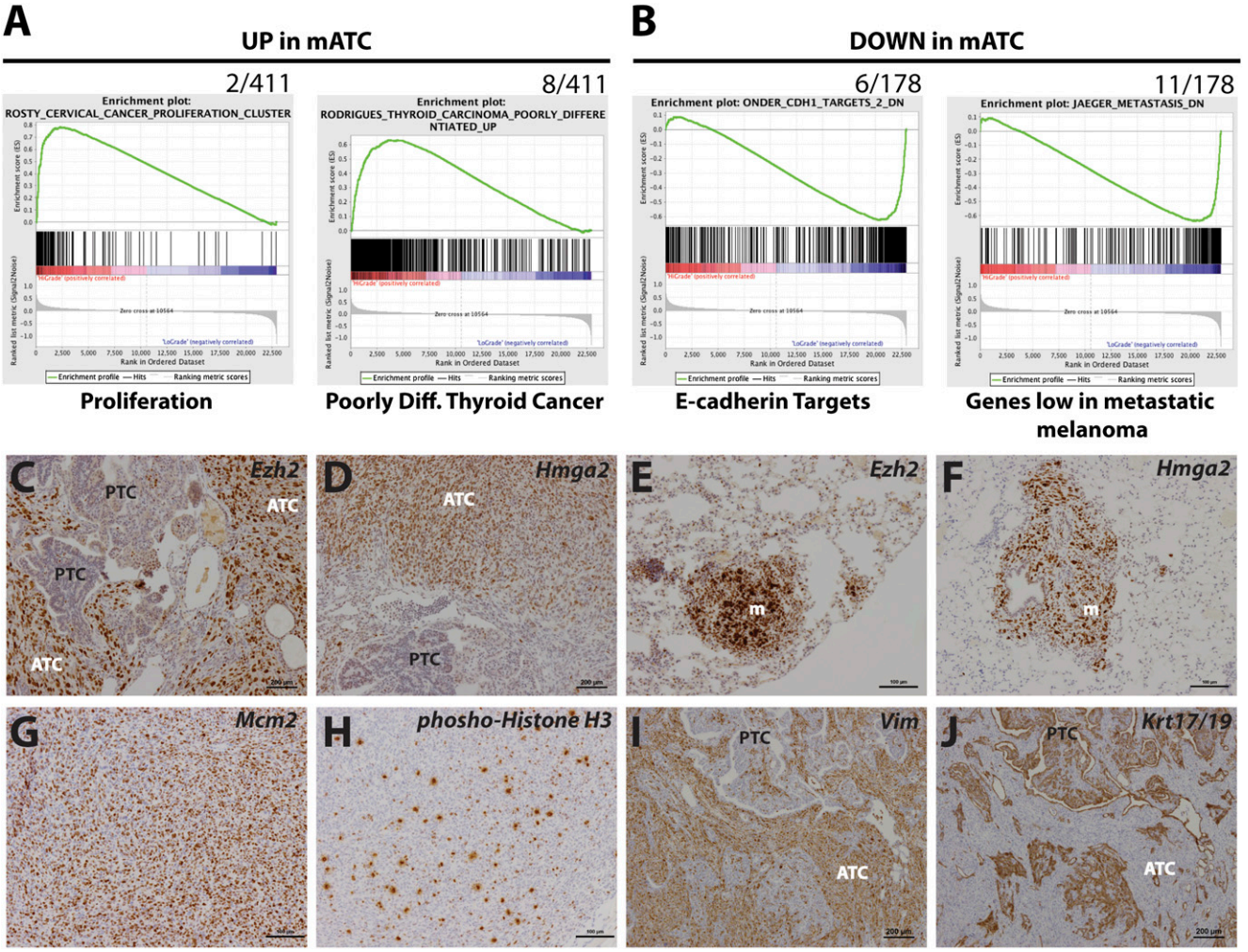

Fig. 4. Gene expression analysis highlights signatures of human ATC. (*A* and *B*) GSEA results showing gene expression signatures of mATC. (*A*) Proliferation and PDTC signatures up-regulated in mATC vs. mPTC. Gene-set rank for each signature shown. (*B*) E-cadherin target genes and genes down-regulated in metastatic vs. primary tumor melanoma strongly down-regulated in mATC. (*C–J*) IHC validation of gene expression signatures. (*E–H*) Elevated Ezh2 (*E*) and Hmga2 (*F*) expression in mATC vs. mPTC tumor components and in lung metastases (*G* and *H*). (*I* and *J*) High proliferation rate in mATC shown by Mcm2 (*I*) staining in which essentially all tumor cells are dividing and by the mitosis marker phospho-histone H3 (*J*). (*K* and *L*) EMT shown by reciprocal staining of vimentin (*K*) in ATC cells and the epithelial cytokeratins 17/19 (*L*) in PTC components. m, metastasis.

Markers of thyroid differentiation and epithelial fate were significantly down-regulated in mATC (Dataset S1, Table S1). Conversely, markers of mesenchymal fate were up-regulated along with embryonic markers, consistent with EMT and marked cellular dedifferentiation evident in human ATC (22, 23). Although EMT and embryonic markers have been associated with stem cell-like properties, we do not believe these data argue for or against a cancer stem cell model in mATC, and additional work would be necessary to address this possibility.

We validated the observed gene expression patterns by IHC using specific antibodies (Fig. 4 *C–J*). Consistent with activation of an embryonic transcriptional signature, the transcriptional regulators enhancer of zeste homolog 2 (Ezh2) and high mobility group AT-hook 2 (Hmga2) were up-regulated in mATC primary tumors and metastases compared with PTC components within the same tumors (Fig. 4 *C–F*). In addition, staining for markers of cell proliferation, minichromosome maintenance complex component 2 (Mcm2) and phospho-histone H3, revealed an extremely high rate of cell division in mATC (Fig. 4 *G* and *H*). Finally, we observed reciprocal expression of the mesenchymal marker vimentin (high in ATC, low in PTC) and the epithelial cytokeratins 17/19 (low in ATC, high in PTC) within tumors harboring both ATC and PTC regions (Fig. 4 *I* and *J*).

We also assessed cellular signaling in mATC. We did not detect increased phospho-Erk staining in ATC components relative to PTC regions in the TBP tumors (Fig. 5*A*). In contrast, examination of PI3K and mammalian target of rapamycin (mTOR) signaling by phospho-specific antibodies demonstrated increased phospho-Akt (S473), and phospho-S6 (S235/236) in ATC compartments (Fig. 5 *B* and *C*). This suggests that these pathways are activated during progression to ATC. Therefore, we sequenced the *Pten* and *phosphatidylinositol 4,5 bisphosphate 3 kinase catalytic subunit alpha* (*Pik3ca*) genes in six mATC tumors for hotspot mutations (*Pik3ca* codons 541–551 and 1041–1051; *Pten* codons 125–135). We detected no mutations at these sites. Epigenetic silencing of Pten has been observed in human ATC and other cancer types (24). Therefore, we performed IHC to determine whether Pten might be silenced

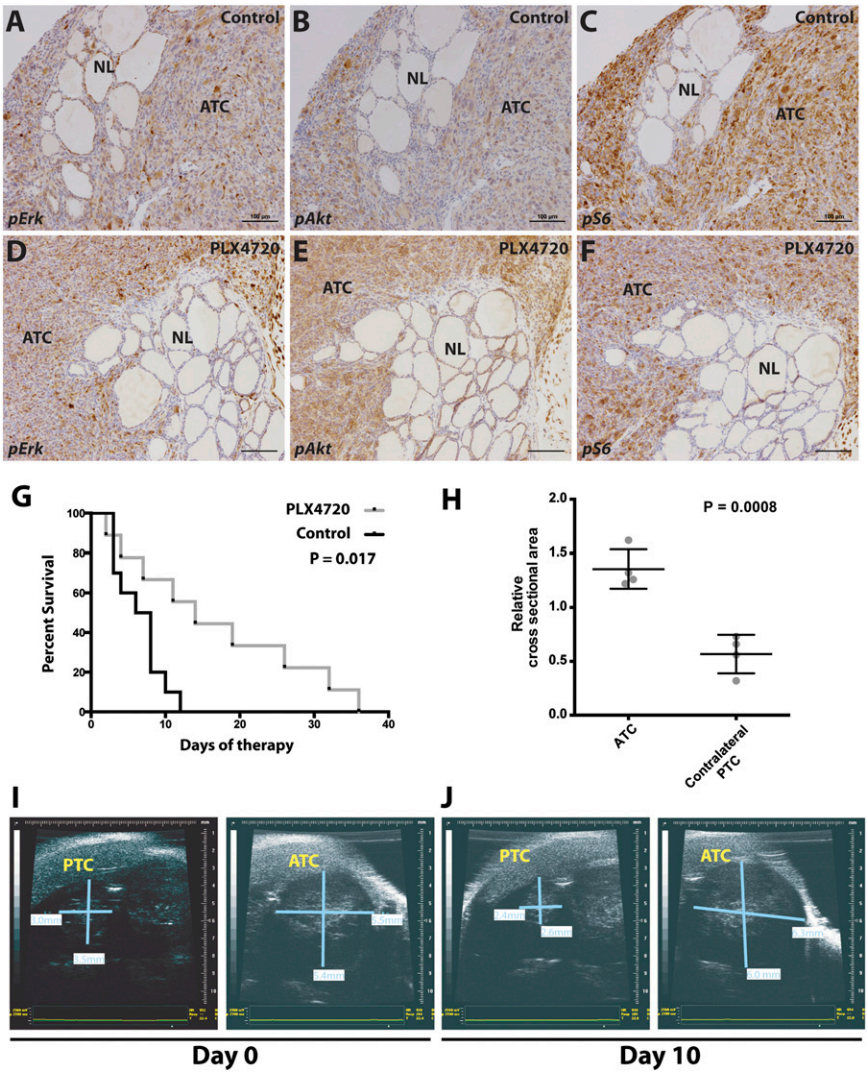

Fig. 5. Incomplete mATC response to BRAF inhibition. (*A–F*) IHC assessment of signaling in control (*A–C*) vs. PLX4720-treated (*D–F*) mATC. Persistent phospho-Erk (Thr202/Tyr204) (*A* and *D*), phospho-Akt (S473) (*B* and *E*), and phospho-S6 (S235/236) in the ATC component but not control normal thyroid tissue in both control and PLX4720-treated tumors. (*G*) Kaplan–Meier plot of control chow vs. PLX4720-treated TBP ATC-bearing animals. (*H*) Relative cross-sectional area of PTC vs. ATC components in three PLX4720-treated ATC-bearing animals. (*I* and *J*) Serial ultrasound images of PLX4720-treated TBP animal. Note the PTC-bearing left thyroid gland exhibits a partial response to treatment whereas the ATC component increases in size during ten days of treatment. NL, normal thyroid.

in TBP mATC. We detected strong expression of Pten in tamoxifen-treated TBP mATC but not control *TPOCreER; Braf*$^{CA/+}$*; Pten*$^{\Delta/\Delta}$ tumors (Fig. S2 *A* and *B*). In addition, we confirmed that Pten is expressed in murine ATC tumor cell lines generated from these animals (Fig. S2*E*). Dissociated mATC tumor cells rapidly proliferated upon placement in culture, and are immortalized as all lines showed no evidence of senescence with serial passaging. Consistent with IHC analysis of TBP mATC tumors in vivo, these lines weakly express Nkx2-1 (Fig. S2*C*). PCR-genotyping of the engineered *Braf*^{CA} and *Trp53* alleles additionally established tumor origin and suggested high tumor purity after 3–7 passages (Fig. S2*D*). These data suggested that activation of PI3K and/or the mTOR pathways occurred by as yet unknown mechanisms in TBP mATC cells. Together, these data suggest that Braf^{V600E} expression in thyroid epithelial cells is sufficient for initiation of PTC, and that loss of p53 function enables progression to highly malignant, lethal ATC that exhibits the cardinal features of human ATC including an embryonic transcriptional program and activation of PI3K and mTOR signaling.

Murine ATCs Respond Incompletely to BRAF Inhibition. A single clinical case report has described a dramatic clinical response in a patient with metastatic ATC to the BRAF inhibitor vemurafenib/PLX4032 (25). However, the recently published experience of a major thyroid cancer referral center with vemurafenib suggests a more modest response (17, 25). Therefore, we developed a preclinical treatment protocol that accounted for the variability in the timing of anaplastic conversion in tumor-bearing TBP animals (Fig. S3*A*). Following tumor induction, TBP cohorts were monitored for a decline in body condition score. At the first sign of a decline in body condition, small-animal ultrasound was performed to assess for the presence of ATC. mATC-bearing animals were then treated with control or PLX4720-compounded chow (PLX4720 is a sister compound to PLX4032/vemurafenib with increased bioavailability in mice). Animals with rapid disease progression and decline in body condition within 48 h were euthanized and excluded from the analysis to ensure adequate absorption of PLX4720. Ultrasound was performed at day zero and every 48 h during treatment to monitor the structural response, and survival was assessed.

Animals receiving PLX4720-compounded chow exhibited a statistically significant survival benefit (Fig. 5*G*; $P = 0.0168$); however, we identified no decrease in the ATC cross sectional area in response to PLX4720. In fact, most tumors grew larger during treatment with PLX4720 (Fig. 5 *I* and *J*). We performed immunohistochemical studies to assess cellular proliferation and apoptosis, and although PLX4720-treated tumors did not exhibit an increase in apoptosis, a slight but statistically significant decrease ($P = 0.02$) in proliferation was identified by phospho-histone H3 staining (Fig. S4*A*). Although this likely contributed to improved survival, we searched for additional factors that might explain the clear improvement in survival of treated animals. Careful review of the imaging results revealed a decrease in contralateral mPTCs present in TBP mice (Fig. 5 *H*–*J*). This suggests that early stage *Braf*-mutant mPTC may be more sensitive to BRAF inhibition, consistent with prior publications in a doxycycline-regulated transgenic BRAF^{V600E} mouse model (9). Because respiratory distress caused by tracheal invasion and compression is the apparent cause of death in tumor-bearing TBP animals, we hypothesized that the decrement in contralateral low-grade PTC components in response to PLX4720 improved the acute upper airway obstruction and therefore survival.

We assessed cellular signaling in PLX4720-treated vs. control mATC by IHC in dissected tumor specimens. Both treated and control tumors exhibited positive phospho-Erk staining, suggesting that MAPK pathway inhibition was incomplete in response to PLX4720 in mATC (Fig. 5 *A* and *D*). In addition, phospho-Akt and phospho-S6 staining was maintained in PLX4720-treated tumors (Fig. 5 *B*, *C*, *E*, and *F*). This is consistent with recently proposed reactivation of upstream receptor-tyrosine kinase that occurred in response to BRAF inhibition in thyroid carcinoma cell lines (16). However, activation of pAkt and pS6 also occurred in untreated tumors. We were technically unable to reliably detect phosphorylated HER3 in treated and untreated tumors, and are therefore unable to determine if HER3 signaling is consistently activated in untreated mATC or in response to PLX4720 treatment. We also performed Western blotting using tumor protein extracts to more accurately quantify MAPK and PI3K signaling; however, we detected no consistent difference between treated and untreated tumors (Fig. S4*B*). This may reflect heterogeneity in the tumor response to PLX4720, or variability in the duration of treatment because animals were euthanized based on body condition rather than at defined time points. Therefore, at this time we cannot determine whether signaling through these pathways is consistently increased or decreased in response to long-term PLX4720 in vivo.

Combined MEK/BRAF Inhibition Enhances Efficacy of MAPK Pathway Targeting in mATC. Treatment of mATC-bearing animals with PLX4720 incompletely suppressed phospho-Erk activity in mATC tumors. The use of combined MEK and BRAF inhibitors in *BRAF*-mutant melanoma has resulted in improved clinical outcomes, suggesting that more potent pathway inhibition may improve efficacy in MAPK pathway mutant cancer cells (26). In addition, the proposed mechanism of BRAF-inhibitor resistance in thyroid carcinoma cells involving the reactivation of upstream receptor tyrosine kinase-driven signaling predicts that downstream MEK inhibition should result in more complete MAPK pathway blockade (16). Therefore, we examined this hypothesis in the mATC model.

Treatment of mATC cells with PLX4720 resulted in incomplete suppression of phospho-Erk activity, consistent with autochthonous TBP mATC tumors (Fig. 6*A*). In contrast, the selective MEK inhibitor PD0325901 more completely suppressed pErk in mATC cells and in the human ATC cell line 8505c. The combination of PD0325901 and PLX4032 resulted in similar pErk levels to PD0325901 alone. In addition, the decrement in pS6 levels roughly correlated with the degree of pErk suppression, suggesting that Braf^{V600E}-mediated signaling impinges upon the mTOR pathway as has been previously suggested (27, 28). We additionally assessed cellular growth of mATC and 8505c cells in response to PLX4032, PD0325901, and the combination of drugs. Consistent with the phospho-Erk response, PD0325901 and combination PD0325901 plus PLX4720 resulted in more complete inhibition of cellular growth in mATC cells vs. PLX4720 alone (Fig. 6*B*).

We next treated a cohort of mATC-bearing animals with PLX4720-compounded and combined PD0325901/PLX4720-compounded chow. To capture mATC outgrowth before significant animal morbidity, tamoxifen-treated TBP animals were monitored with weekly ultrasound imaging (Fig. S3*B*). Upon detection of ATC, animals were randomly assigned to receive PLX4720-compounded or PLX4720 plus PD0325901-compounded chow. Consistent with results obtained in cultured cells, we observed a dramatic response to combined PLX4720/PD0325901 administration compared with PLX4720 monotherapy (Fig. 6 *C* and *D*). Combination-treated animals exhibited an enhanced tumor response, including complete regression in three of four mATC-bearing animals, and significantly prolonged survival ($P = 0.0246$) (Fig. 6 *E* and *F*). We have not assessed the response of mATC to single agent MEK inhibitors in vivo; therefore, we cannot determine whether the antitumor effect in combination treated animals was due to enhanced efficacy of downstream MEK inhibition or to the combined impact of these drugs. The response of mATC and 8505c cells in

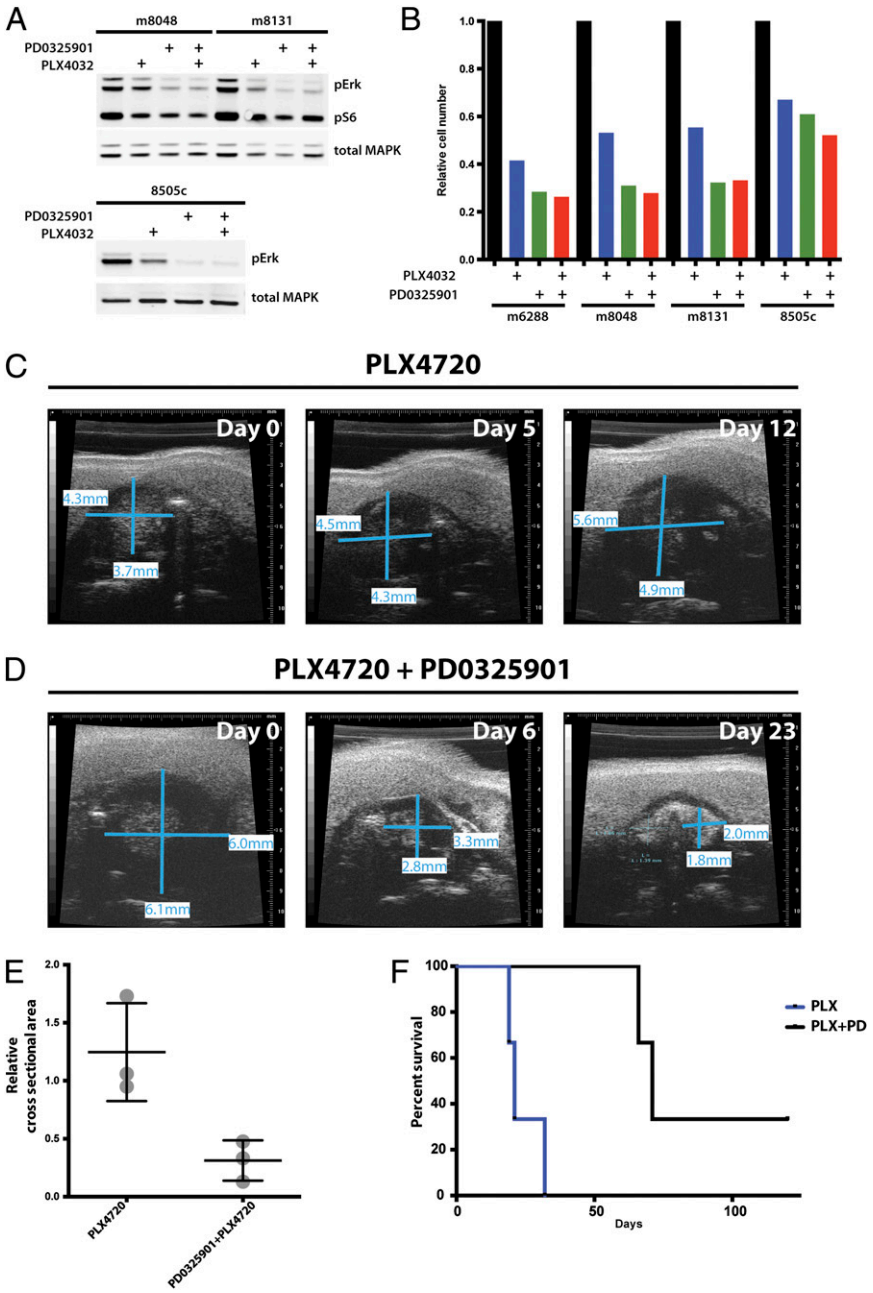

Fig. 6. Combined BRAF and MEK inhibition improves therapeutic response in ATC. (*A*) Western blot of murine ATC (m8048, m8131) and human (8505c) cell lines showing phospho-Erk (Thr202/Tyr204) and phospho-S6 (S235/236) response to PLX4720, PD0325901, and combination treatment. (*B*) Relative cell number 72 h following drug administration to murine (m6288, m8048, and m8131) and human ATC (8505c) cells. (*C*) Ultrasound imaging of PLX4720-treated TBP animal demonstrating growth of ATC during treatment. (*D*) PLX4720 plus PD0325902-treated TBP animal showing rapid tumor regression upon administration of compounded diet. (*E*) Relative cross-sectional area of PLX4720-treated and PLX4720 plus PD0325901-treated ATC tumors. Cross-sectional area was measured at day 0 and 2 wk following initiation of compounded diet. (*F*) Overall survival of PLX4720-treated and PLX4720 plus PD0325901-treated animals ($P = 0.0246$).

culture suggests that the majority of the effect may be achieved by PD0325901. However, these results establish that more complete MAPK blockade enhances antitumor effect in ATC cells and tumors.

Discussion

We describe here a previously lacking autochthonous, genetically engineered mouse model of *BRAF* mutant ATC and demonstrate that this model recapitulates the cardinal features of the human disease, including underlying genetics, rapid clinical progression, histomorphology, gene expression signatures, and intrinsic resistance to selective BRAF inhibition. We also demonstrate that more complete MAPK pathway blockade improves therapeutic responses in cultured ATC cell lines and autochthonous tumors.

Multistep Thyroid Carcinogenesis. Mouse models have largely confirmed the role of *BRAF* mutation as an initiator of thyroid carcinogenesis (9, 10, 12). However, these models have been technically limited by embryonic expression of $BRAF^{V600E}$

and/or supraphysiologic circulating TSH levels that can promote thyroid cellular growth. In addition, there has recently been controversy regarding whether $BRAF^{V600E}$ is sufficient to induce PTC in the adult murine thyroid gland and whether $BRAF^{T1799A}$ mutation is a clonal event in human PTC (29, 30). Although we believe the preponderance of experimental data supports the role of BRAF as an initiating genetic event, our results are the strongest to date that mosaic $BRAF^{V600E}$ expression in the adult murine thyroid is sufficient to initiate PTC. The fact that PTC is not observed in corn oil-treated TB animals 12 wk after induction, and all tamoxifen-treated TB animals harbor PTC, strongly argues for the sufficiency of $BRAF^{V600E}$ to initiate PTC in the adult. In addition, in contrast to Shimamura et al. (30), we have successfully induced PTC in $Braf^{CA/+}$ animals by surgical delivery of Cre-expressing adenovirus.

Analyses of human ATC specimens have consistently implicated p53 as an important tumor suppressor during thyroid cancer progression. *TP53* mutations are detected at high frequency in ATCs, at lower frequency in PDTC, and uncommonly in PTCs (5, 6). In addition, prior work from a mouse model of PTC driven by transgenic overexpression of a *RET/PTC* fusion has implicated p53 loss in progression from papillary to PDTC and possibly ATC (13). Our data demonstrate that combined *BRAF* mutation and loss of p53 cooperate in vivo to facilitate progression to ATC. Interestingly, although loss of p53 appears to be required for progression to ATC, our data suggest that additional events may be required for ATC conversion. Firstly, the ∼6-mo latency after induction of $Braf^{V600E}$ expression and p53 loss suggests this combination of events is insufficient to direct the complete ATC phenotype. In addition, the slow temporal progression of TBP tumors followed by sudden ATC outgrowth as assessed by serial ultrasound imaging is consistent with acquired somatic genetic or epigenetic alterations driving tumor progression and conversion to the anaplastic phenotype. The mouse model described here provides an ideal autochthonous platform to begin to dissect the molecular mechanisms of this transition.

Recently, a genetically engineered mouse model of follicular thyroid carcinoma progression to ATC was generated by compound deletion of p53 and Pten in the murine thyroid follicular epithelium (14). The *TPOCre;* $Pten^{\Delta/\Delta}$*;* $p53^{\Delta/\Delta}$ animals develop invasive, undifferentiated carcinoma with sarcomatoid features. Although this model exhibits a longer ATC latency, the histologic phenotype is indeed quite similar to the features we detect in the TBP model. This may support the notion that each of these models acquires convergent events such that the TBP model activates the PI3K pathway, and *TPOCre;* $Pten^{\Delta/\Delta}$*;* $p53^{\Delta/\Delta}$ animals acquire MAPK pathway alterations. However, genotyping for *Ras* family hotspot mutations was negative in *TPOCre;* $Pten^{\Delta/\Delta}$*;* $p53^{\Delta/\Delta}$ tumors (14). Conversely, we detected no *Pten* or *Pik3ca* hotspot mutations in TBP mATC tumors, and these tumors maintained expression of Pten, as assessed by IHC. This suggests that neither MAPK nor PIK3CA alterations are essential for anaplastic conversion. However, other acquired mechanisms of activating the PI3K pathway in the TBP mATC model have not been excluded. Together, these models provide strong in vivo evidence for the important role of p53 loss and PI3K pathway activation during progression to ATC.

Response of ATC to MAPK Inhibition. Previous studies using MAPK pathway inhibitors in ATC had relied upon highly passaged human ATC cells in culture or transplanted into immunocompromised mice (16, 31, 32). Our results demonstrating an incomplete response of mATCs to PLX4720 are consistent with the reduced sensitivity of a variety of human thyroid carcinoma cell lines to MAPK pathway inhibition in cultured conditions. Relief of negative feedback to the HER3 receptor tyrosine kinase signaling pathway has been implicated as a mechanism of intrinsic resistance of ATC cells in culture (16). This mechanism predicts that downstream MEK inhibition may blunt reactivation of MAPK signaling. Upstream RTK activation may also impinge upon the PI3K/Akt pathway, suggesting that MAPK inhibition may be insufficient to suppress growth and/or survival of BRAF-mutant thyroid carcinoma cells.

Our data both in vitro and in vivo, however, suggest that potent MAPK blockade may be sufficient for a robust initial antitumor response. mATC tumors also exhibit increased signaling through the PI3K/Akt pathway, and although the response to combination PLX4720/PD0325901 was robust in our study, mATC tumors eventually recurred. Human ATCs also harbor frequent alterations in the PI3K pathway (4). Therefore, it will be important to determine whether combined MAPK/PI3K inhibition will improve outcomes in this model system, as has been suggested from studies in several cancer types (33). It will also be interesting to interrogate the mechanisms underlying tumor recurrence following combined BRAF and MEK inhibition in this model. The data presented here, however, strongly argue for a central role of MAPK pathway inhibitors in treatment regimens for patients with advanced forms of thyroid cancer and suggest that more potent pathway blockade may result in improved responses.

Mouse Models for Uncommon Aggressive Tumors. A lack of available tissue and participants in clinical trials has hampered scientific progress and therapeutic improvements for many uncommon tumors, particularly those exhibiting highly aggressive clinical behavior. Using the somatic genetics of human ATC, we describe a valid preclinical mouse model recapitulating the temporal progression, gene expression programs, and resistance to targeted BRAF inhibitors seen in human thyroid carcinoma. We propose this model as a suitable experimental platform from which to begin to genetically dissect the molecular determinants of ATC progression and resistance to therapies.

Methods

Cloning and Generation of TPOCreER Mice. The TPOCre vector was provided by Shioko Kimura (National Cancer Institute, Bethesda, MD) (18). A partial SalI plus MluI digest was performed to remove the Cre coding sequence. This was replaced by a PCR-generated CreER (T2) ORF flanked by SalI and MluI restriction sites. Restriction mapping and DNA sequencing confirmed all cloning junctions. TPOCreER expression construct was excised with KpnI and injected into fertilized oocytes using standard techniques. Two independent transgenic animals were generated. One founder strain (1139) was used for all experiments described in this paper.

Animal Studies. All studies were performed under an Institutional Animal Care and Use Committee- and Massachusetts Institute of Technology Committee on Animal Care-approved animal protocol. TPOCreER animals were crossed to the previously described mouse strains available from The Jackson Laboratory: $Braf^{tm1Mmcm}$/J (stock no. 017837), $Gt(ROSA)26Sor^{tm9(CAG\_tdTomato)Hze}$/J (stock no. 007909), $Trp53^{tm1Brn}$/J (stock no. 008462), and $Trp53^{tm3.1Tyj}$/J (stock no. 008182). All mice were maintained on a mixed C57BL/6; 129SvJae background. Genotyping primers and protocols are available upon request. Tumor induction was performed by i.p. administration of 0.1–0.2 mg/g tamoxifen dissolved in corn oil (Sigma) for one or two administrations at age 8–12 wk. Ad5-CMV-Cre was obtained from the University of Iowa Gene Transfer Vector Core Facility. PLX4720 and PD0325901 were administered in compounded chow from Research Diets. PLX4720 was administered at 400 ppm in the initial monotherapy trial (Fig. S2*A*) and at 200 ppm in the combination trial (Fig. S2*B*). PD0325901 was administered at 7 ppm in diet. A Vevo 770 small-animal ultrasound with a 704 probe was used to image thyroid tumors for treatment studies. Cross-sectional area was calculated by measuring maximal anterior-posterior and left-right dimension using the standard area for an ellipse. GraphPad Prism 5.0 or 6.0 was used for all statistical analyses. All survival *P* values were calculated using a log-rank (Mantel–Cox) test.

Hormone Measurements. Blood was collected from male and female mice by retro-orbital bleeding and allowed to clot at room temperature for 1 h and

then centrifuged. Serum was stored at −80 °C until assays were performed. Samuel Refetoff (University of Chicago, Chicago, IL) performed TSH and T4 measurement, as previously described, on a fee-for-service agreement (34).

Gene Expression Analyses. Total RNA was harvested from five snap-frozen TB/+ (PTC) and TBP tumors after histological confirmation of papillary or anaplastic phenotype. Affymetrix Mouse Exon 1.0 ST arrays were used as previously described. Raw hybridization intensities from Affymetrix Mouse Gene 1.0 ST arrays were normalized and summarized using the open-source Affymetrix Power Tools software package (Affymetrix) to derive gene-level expression estimates. Multiple probe sets targeting the same gene were collapsed using their median value in order to eliminate duplicates from the dataset. Differential gene expression analysis was performed using the limma package in the R environment for statistical computing (www.r-project.org and ref. 35). GSEA was performed with GSEA software and the molecular signature database (MSigDB) (21). Gene expression datasets have been deposited in the National Center for Biotechnology Information Gene Expression Omnibus database (accession no. GSE55933).

IHC. See Dataset S1, Table S2 for a list of antibodies used in this study. IHC was performed using standard protocols on a ThermoFisher Lab Vision Autostainer 360.

Cell Line Studies. mATC tumors were dissociated by mincing freshly dissected tumors and digestion in HBSS-free with 100 μL of trypsin (0.25%), 200 μL of Dispase (BD), and 100 μL of collagenase (10 mg/mL; Worthington) for 30 min to 1 h. Following incubation and filtering through a 40- to 100-μm cell strainer, dissociated cells were plated on to tissue culture dishes in DMEM supplemented with 10% FBS and pen/strep. Cells were passaged and frozen using standard techniques. Human 8505c cells were obtained from the laboratory of Sareh Parangi (Massachusetts General Hospital). PD0325901 was added to media to a final concentration of 50 nM, and PLX4720 was supplemented to 2 μM in all experiments. Protein extracts were harvested after 24 h of incubation in drug vs. vehicle (DMSO) media using radioimmunoassay immunoprecipitation assay buffer supplemented with protease and phosphatase inhibitors (Roche). See Dataset S1, Table S2 for a list of antibodies used in this study. Cell number was assessed 72 h following addition of drug or DMSO using the Celltiter-Glo kit (Promega).

Note Added in Proof. Separately, Charles et al. demonstrated that combined expression of BRAF(V600E) with silencing of PTEN also elicits anaplastic thyroid cancer in a related mouse model (36).

ACKNOWLEDGMENTS. We thank Plexxikon for providing PLX4720 and PD0325901 for experiments, Dr. Shioko Kimura [National Cancer Institute (NCI)] for providing the TPOCre plasmid, Dr. Samuel Refetoff (University of Chicago) for mouse TSH and T4 assays, Dr. Sareh Parangi (Massachusetts General Hospital) for sharing 8505c human ATC cells, and Kaitlyn Sanders for technical assistance. We thank Thales Papagiannakopoulos, Tuomas Tammela, Eric Snyder, and Gilbert H. Daniels for critical review of the manuscript. This work was supported by the Howard Hughes Medical Institute (T.J.), National Institutes of Health R01CA131261 (to M.M.), and an American Thyroid Association research award (to D.M.). D.M. is supported by NCI Career Development Award K08CA160658.

1. Cooper DS, et al.; American Thyroid Association (ATA) Guidelines Taskforce on Thyroid Nodules and Differentiated Thyroid Cancer (2009) Revised American Thyroid Association management guidelines for patients with thyroid nodules and differentiated thyroid cancer. *Thyroid* 19(11):1167–1214.
2. Smallridge RC, et al.; American Thyroid Association Anaplastic Thyroid Cancer Guidelines Taskforce (2012) American Thyroid Association guidelines for management of patients with anaplastic thyroid cancer. *Thyroid* 22(11):1104–1139.
3. Ricarte-Filho JC, et al. (2009) Mutational profile of advanced primary and metastatic radioactive iodine-refractory thyroid cancers reveals distinct pathogenetic roles for BRAF, PIK3CA, and AKT1. *Cancer Res* 69(11):4885–4893.
4. Santarpia L, El-Naggar AK, Cote GJ, Myers JN, Sherman SI (2008) Phosphatidylinositol 3-kinase/akt and ras/raf-mitogen-activated protein kinase pathway mutations in anaplastic thyroid cancer. *J Clin Endocrinol Metab* 93(1):278–284.
5. Fagin JA, et al. (1993) High prevalence of mutations of the p53 gene in poorly differentiated human thyroid carcinomas. *J Clin Invest* 91(1):179–184.
6. Ito T, et al. (1992) Unique association of p53 mutations with undifferentiated but not with differentiated carcinomas of the thyroid gland. *Cancer Res* 52(5):1369–1371.
7. Nikiforov YE, Nikiforova MN (2011) Molecular genetics and diagnosis of thyroid cancer. *Nat Rev Endocrinol* 7(10):569–580.
8. Gauchotte G, et al. (2011) BRAF, p53 and SOX2 in anaplastic thyroid carcinoma: Evidence for multistep carcinogenesis. *Pathology* 43(5):447–452.
9. Chakravarty D, et al. (2011) Small-molecule MAPK inhibitors restore radioiodine incorporation in mouse thyroid cancers with conditional BRAF activation. *J Clin Invest* 121(12):4700–4711.
10. Charles RP, Iezza G, Amendola E, Dankort D, McMahon M (2011) Mutationally activated BRAF(V600E) elicits papillary thyroid cancer in the adult mouse. *Cancer Res* 71(11):3863–3871.
11. Franco AT, et al. (2011) Thyrotrophin receptor signaling dependence of Braf-induced thyroid tumor initiation in mice. *Proc Natl Acad Sci USA* 108(4):1615–1620.
12. Knauf JA, et al. (2005) Targeted expression of BRAFV600E in thyroid cells of transgenic mice results in papillary thyroid cancers that undergo dedifferentiation. *Cancer Res* 65(10):4238–4245.
13. La Perle KM, Jhiang SM, Capen CC (2000) Loss of p53 promotes anaplasia and local invasion in ret/PTC1-induced thyroid carcinomas. *Am J Pathol* 157(2):671–677.
14. Antico Arciuch VG, et al. (2011) Thyrocyte-specific inactivation of p53 and Pten results in anaplastic thyroid carcinomas faithfully recapitulating human tumors. *Oncotarget* 2(12):1109–1126.
15. Sherman SI (2011) Targeted therapies for thyroid tumors. *Mod Pathol* 24(Suppl 2): S44–S52.
16. Montero-Conde C, et al. (2013) Relief of feedback inhibition of HER3 transcription by RAF and MEK inhibitors attenuates their antitumor effects in BRAF-mutant thyroid carcinomas. *Cancer Discov* 3(5):520–533.
17. Kim KB, et al. (2013) Clinical responses to vemurafenib in patients with metastatic papillary thyroid cancer harboring BRAF(V600E) mutation. *Thyroid* 23(10):1277–1283.
18. Kusakabe T, Kawaguchi A, Kawaguchi R, Feigenbaum L, Kimura S (2004) Thyrocyte-specific expression of Cre recombinase in transgenic mice. *Genesis* 39(3):212–216.
19. Dankort D, et al. (2007) A new mouse model to explore the initiation, progression, and therapy of BRAFV600E-induced lung tumors. *Genes Dev* 21(4):379–384.
20. Orim F, et al. (2014) Thyrotropin signaling confers more aggressive features with higher genomic instability on BRAF(V600E)-induced thyroid tumors in a mouse model. *Thyroid* 24(3):502–510.
21. Subramanian A, et al. (2005) Gene set enrichment analysis: A knowledge-based approach for interpreting genome-wide expression profiles. *Proc Natl Acad Sci USA* 102(43):15545–15550.
22. Knauf JA, et al. (2011) Progression of BRAF-induced thyroid cancer is associated with epithelial-mesenchymal transition requiring concomitant MAP kinase and TGFβ signaling. *Oncogene* 30(28):3153–3162.
23. Wenig BM (1993) *Atlas of Head and Neck Pathology* (Saunders, Philadelphia).
24. Hou P, Ji M, Xing M (2008) Association of PTEN gene methylation with genetic alterations in the phosphatidylinositol 3-kinase/AKT signaling pathway in thyroid tumors. *Cancer* 113(9):2440–2447.
25. Rosove MH, Peddi PF, Glaspy JA (2013) BRAF V600E inhibition in anaplastic thyroid cancer. *N Engl J Med* 368(7):684–685.
26. Flaherty KT, et al. (2012) Combined BRAF and MEK inhibition in melanoma with BRAF V600 mutations. *N Engl J Med* 367(18):1694–1703.
27. Faustino A, et al. (2012) mTOR pathway overactivation in BRAF mutated papillary thyroid carcinoma. *J Clin Endocrinol Metab* 97(7):E1139–E1149.
28. Jin N, Jiang T, Rosen DM, Nelkin BD, Ball DW (2011) Synergistic action of a RAF inhibitor and a dual PI3K/mTOR inhibitor in thyroid cancer. *Clin Cancer Res* 17(20): 6482–6489.
29. Guerra A, et al. (2012) The primary occurrence of BRAF(V600E) is a rare clonal event in papillary thyroid carcinoma. *J Clin Endocrinol Metab* 97(2):517–524.
30. Shimamura M, et al. (2013) Postnatal expression of BRAFV600E does not induce thyroid cancer in mouse models of thyroid papillary carcinoma. *Endocrinology* 154(11):4423–4430.
31. Nehs MA, et al. (2012) Late intervention with anti-BRAF(V600E) therapy induces tumor regression in an orthotopic mouse model of human anaplastic thyroid cancer. *Endocrinology* 153(2):985–994.
32. Nucera C, et al. (2011) Targeting BRAFV600E with PLX4720 displays potent antimigratory and anti-invasive activity in preclinical models of human thyroid cancer. *Oncologist* 16(3):296–309.
33. Wong KK, Engelman JA, Cantley LC (2010) Targeting the PI3K signaling pathway in cancer. *Curr Opin Genet Dev* 20(1):87–90.
34. Pohlenz J, et al. (1999) Improved radioimmunoassay for measurement of mouse thyrotropin in serum: Strain differences in thyrotropin concentration and thyrotroph sensitivity to thyroid hormone. *Thyroid* 9(12):1265–1271.
35. Gentleman RC, et al. (2004) Bioconductor: Open software development for computational biology and bioinformatics. *Genome Biol* 5(10):R80.
36. Charles RP, Silva J, Iezza G, Phillips W, McMahon M (2014) BRAF(V600E) cooperates with PIK3CA(H1074R) to promote anaplastic thyroid carcinogenesis. *Mol Cancer Res*, in press.